How do cormorants counter buoyancy during submerged swimming?

Gal Ribak[1], Daniel Weihs[2] and Zeev Arad[1],*

[1]*Faculty of Biology, Technion – Israel Institute of Technology, Israel* and [2]*Faculty of Aerospace Engineering, Technion – Israel Institute of Technology, Haifa 32000, Israel*

*Author for correspondence (e-mail: zarad@tx.technion.ac.il)

Summary

Buoyancy is a de-stabilizing force for diving cormorants that forage at shallow depths. Having to counter this force increases the cost of transport underwater. Cormorants are known to be less buoyant than most water birds but are still highly buoyant (ρ=~0.8 kg m^{-3}) due to their adaptations for aerial flight. Nevertheless, cormorants are known to dive at a wide range of depths, including shallow dives where buoyancy is maximal. We analyzed the kinematics of underwater swimming of the great cormorant (*Phalacrocorax carbo sinensis*) in a shallow pool to discover and evaluate the mechanisms countering buoyancy while swimming horizontally. The birds maintained a very uniform cyclic paddling pattern. Throughout this cycle, synchronized tilting of the body, controlled by the tail, resulted in only slight vertical drifts of the center of mass around the average swimming path. We suggest that this tilting behavior serves two purposes: (1) the elongated bodies and the long tails of cormorants, tilted at a negative angle of attack relative to the swimming direction, generate downward directed hydrodynamic lift to resist buoyancy and (2) during the propulsive phase, the motion of the feet has a significant vertical component, generating a vertical component of thrust downward, which further helps to offset buoyancy. The added cost of the drag resulting from this tilting behavior may be reduced by the fact that the birds use a burst-and-glide pattern while swimming.

Key words: buoyancy, diving, kinematics, underwater, cormorant, *Phalacrocorax*.

Introduction

Air-breathing divers are limited not only by a limited oxygen supply, and by pressure changes with depth (Boyd, 1997; Butler, 2001; Jones et al., 1988), but also by the need to carry air volumes underwater. These air volumes increase buoyancy by reducing the overall body density, hence the diver has to face a hydrostatic force acting to push it toward the surface (Alexander, 1968; Fish et al., 2002; Lovvorn et al., 1991; Stephenson, 1993; Taylor, 1994; Webb et al., 1998). Air-breathing divers demonstrate a wide variety of adaptations to pelagic life that also reduce the buoyancy of the body. These include exhaling of air prior to the dive (ducks and penguins – Butler and Woakes, 1979; Lovvorn, 1991; Sato et al., 2002; sea turtles – Hochscheid et al., 2003), heavy skeletons (sirenians – Domning and Buffrénil, 1991) and blubber instead of fur for insulation (cetaceans *vs* semiaquatic mammals – Fish, 2000; Fish et al., 2002). Apart from these hydrostatic adjustments, fast swimmers can rely on dynamic buoyancy control by using control surfaces (fins) that are positioned at a distance from the center of mass and generate a hydrodynamic lift force (Webb and Weihs, 1983). This force is perpendicular to the swimming direction and therefore may be used to correct for sinking/floating and thus maintain a horizontal course (Alexander, 1968, 1990; Webb and Weihs, 1983). Resisting buoyancy (negative or positive) while swimming horizontally can also be accomplished by actively directing propulsive force up or down against buoyancy (Alexander, 1990; Lovvorn et al., 1991).

Buoyancy has especially severe implications for diving birds because the primary anatomic adaptations of birds are for flying. Low body density and large air volumes (in the respiratory tract and in the plumage) aid birds in reducing flight costs, resulting in increased buoyancy and thus increased diving cost (Lovvorn and Jones, 1994; Wilson et al., 1992). It has been estimated that, during vertical dives (dives to the bottom and back), ducks invest up to 95% of the mechanical work generated by the feet against buoyancy (Stephenson et al., 1989). In birds that dive in search and pursuit of prey (horizontal divers), buoyancy acts at a perpendicular direction to the swimming direction and hence acts as a de-stabilizing force. Wilson et al. (1992) and Lovvorn and Jones (1991) showed that horizontal diving birds are relatively less buoyant than surface swimming or vertical diving birds, probably due to reduced plumage air volume. Another relatively simple way to reduce the effect of buoyancy without increasing flying cost is to dive to depths where ambient pressure compresses the air volumes of the body (Hustler, 1992; Lovvorn et al., 1999; Wilson et al., 1992). Both of the above mechanisms seem to apply to some

cormorant species, as cormorants have a reduced plumage layer that presumably contains less air (Lovvorn and Jones, 1991; Wilson et al., 1992), and telemetry and diet studies of free-ranging cormorants have shown that foraging focuses on benthic prey (Gremillet and Wilson, 1999; Kato et al., 2000; Wanless et al., 1992). However, cormorants are opportunistic hunters, attracted to areas of high prey density, and demonstrate high variability of dive sites and dive depths (Boldreghini et al., 1997; Gremillet et al., 1998). Cormorants are especially interesting in the sense that they seem to master both flying and submerged swimming. Although higher than that of surface-feeding birds, the specific weights of cormorants, measured in carcasses (Wilson et al., 1992) and in forcibly submerged live birds (Lovvorn and Jones, 1991), are still considerably low (~0.8×10^3 kg m^{-3}). This means that unless the actual specific weight of voluntary diving cormorants is much higher, shallow-diving cormorants are still required to invest considerable work against buoyancy.

Cormorants swim underwater by synchronized feet propulsion, with the wings tightly folded close to the body (Schmid et al., 1995). The shape of the body is streamlined, with no specific control surfaces. This reduces the drag on the body but renders control of destabilizing forces more difficult than for shapes with fins and/or other control surfaces. Previous studies considered feet propulsion to be drag-based, as the thrust is generated by kicking the feet backwards, in the opposite direction to the moving body (Baudinette and Gill, 1985). However, recent reports (Johansson and Lindhe Norberg, 2000, 2001; Johansson and Norberg, 2003) have shown that the trajectory and the angle of attack (AoA) of the feet in cormorants, grebes and perhaps other foot-propelled birds are consistent with hydrodynamic lift-based propulsion, at least for the later parts of the stroke. This is because the feet move backwards at about the same speed as the swimming speed of the body and hence have an almost zero horizontal speed compared with still water, while there is a large vertical speed component to the feet trajectory. Thus, hydrodynamic lift may be the major thrust-contributing force in foot propulsion. In the case of the cormorant, the trajectory of the feet during the stroke also suggests a significant vertical force component that can be used to oppose the positive buoyancy.

The question remains: how do cormorants manage to efficiently divide their power output between forward thrust and the maintenance of vertical stability during shallow, straight, horizontal dives?

Here, we study the underwater swimming kinematics of the great cormorant (*Phalacrocorax carbo sinensis*), emphasizing the balance of forces in the vertical direction. The buoyancy of the cormorant, as in other birds, is relatively high for a submerged swimmer (ρ=~0.8 kg m^{-3}), suggesting the use of specific mechanisms to remain submerged during underwater horizontal swimming. Specifically, we tested the contribution of hydrodynamic lift of the body and the tail as well as feet propulsion to offset effects of buoyancy during horizontal submerged swimming.

Materials and methods

Research animals

Experiments were conducted on four male and five female adult great cormorants *Phalacrocorax carbo sinensis* Blumelbach 1798 (age >3 years). Seven of the birds were obtained as chicks and hand-reared in captivity, while the other two were wild cormorants captured under permit. The birds were obtained and held under license from the Israel Nature and National Parks Protection Authority (permit number 2001/10965). All experiments were approved by the Committee for the Supervision of Animal Experiments (permit number IL-080-11-2001). The birds were held in a large open aviary (5.4×6×6 m) with free access to water for swimming. They were fed a fish mixture of *Cyprinus carpio* and *Tilapia* spp. *ad libitum*. Body mass was measured once a month to ensure all were feeding properly and to monitor seasonal and growth-associated mass changes.

All animals were trained by rewarding desired behavior with a fish. The animals were trained to perform the following routine: (1) step on an electronic balance, (2) enter the pool used for the experiments through a small window (50×50 cm) connecting the pool with the aviary and (3) dive inside a mesh channel placed on the floor of the pool (see description below). Training lasted two weeks at the most, after which all birds were repeating the desired tasks in response to a vocal or a visual signal from the trainer.

Morphometrics of carcasses

Body mass, density (buoyancy), the position of the center of mass, and dimensions of the body, tail and feet were measured on carcasses of wild cormorants shot over fishing ponds as part of a wildlife management program. Less than two hours elapsed from shooting to freeze-storage of the carcasses. Measurements were conducted after fully defrosting the birds at room temp (~18°C). Density was measured using the displacement volume technique (Lovvorn and Jones, 1991; Wilson et al., 1992) with the following modification. We lowered the carcass (head first) at a 45° angle and placed it horizontally on the bottom of a flat tank (40×30 cm), filled with 40 cm of water up to a small outlet tube. The water displaced by the carcass was collected and weighed to the nearest 1 g. Measurements lasted 3-4 min, during which the carcass was submerged. We made no correction for air lost from the plumage during that time or for the air volume in the air sacs. We did, however, seal the throat of the carcass with a cable tie prior to the measurement to prevent air loss from the trachea during submergence. We chose to measure the carcass horizontally since we were interested in measuring the buoyancy of the carcasses at shallow depths. Performing the measurement in a horizontal position, rather than vertically (see Lovvorn and Jones, 1991), ensured minimal compression of the plumage air and decreased the pressure gradient over the long axis of the body, which might facilitate air loss from the plumage. To fit the carcass horizontally in the tank, the neck was folded backward alongside the body. The position of the center of mass along the long axis of the body was found by

laying the carcass (neck stretched) on a flat 1×0.1 m rod, balanced on a swiveling pole (diameter 7 cm). By sliding the carcass toward one end of the rod, the position of the point of balance (distance from the tip of the bill) was found and marked. We assumed that the center of mass is located on the body midline due to bilateral symmetry. We made no attempts to measure the exact dorso-ventral position of the center of mass due to the limitation of the technique.

The cormorant carcasses were positively buoyant. As a result, underwater, the point where pitch moments are balanced along the longitudinal axis of the body is determined by the position of the center of mass and the center of buoyancy (Webb and Weihs, 1994). We termed this point 'center of vertical static stability'. To find the position of the center of vertical static stability of the carcasses we repeated the procedure in a 30 cm-deep pool where the carcass and apparatus were completely submerged. The carcass was

secured to the apparatus by three fixed metal cables (same length). The cables pressed the carcass toward the rod at distances 0 and ±25 cm from the center of rotation. The apparatus was carefully brushed of air bubbles prior to the underwater measurements.

The position of the center of mass on the body of the carcasses was allometrically applied to the live trained birds, based on their body length. Similarly, buoyancy of the trained birds was estimated based on their body mass.

The planar area of the left foot of 22 carcasses was measured from photographs. The feet in the photographs were fixed to an angle of 110° between digits IV and I (Fig. 1A), similar to the shape of the foot during paddling observed in our trained birds (110±6°; mean ± s.e.m.; N=9 birds). We defined the span of the foot as the maximal projection of the plan of the foot (between digits I and IV) on the lateral proximal/distal axis of the bird (the direction perpendicular to the swimming direction). During the stroke, the foot and the tarsusmetatarsus (TMT) were oriented laterally at an angle of 16±2° (N=9 birds) away from the midline of the body (and the swimming direction). To account for this change in foot orientation relative to the motion in the backward and upward directions, the span measurement was preformed with the left foot rotated at 16° clockwise (see Fig. 1A). The foot is a thin surface and, as such, has a significant added mass (the mass of water accelerated with the foot) only at high AoAs. To calculate the
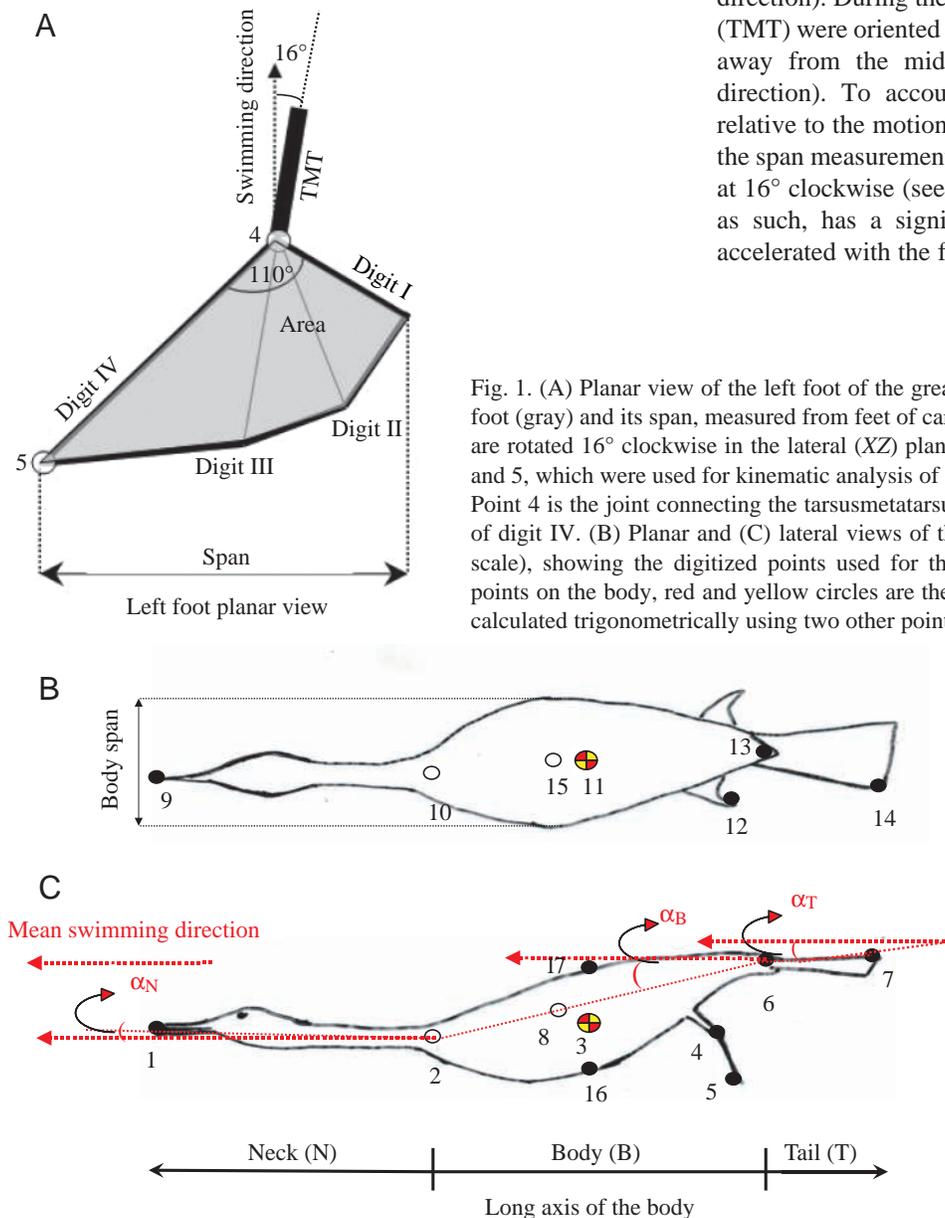

Fig. 1. (A) Planar view of the left foot of the great cormorant showing the webbed area of the foot (gray) and its span, measured from feet of carcasses. The feet and tarsusmetatarsus (TMT) are rotated 16° clockwise in the lateral (*XZ*) plane during the stroke. Also shown are points 4 and 5, which were used for kinematic analysis of the foot motion in the trained birds (see text). Point 4 is the joint connecting the tarsusmetatarsus (TMT) with the foot, and point 5 is the tip of digit IV. (B) Planar and (C) lateral views of the great cormorant during swimming (not to scale), showing the digitized points used for the kinematic analysis. Black dots are actual points on the body, red and yellow circles are the glued tags, and the empty circles are points calculated trigonometrically using two other points. Points visible in lateral view are: tip of the bill (1), base of the neck (2), mid-body (3), base of the foot (4), tip of digit IV (5), base of the tail (6), tip of the tail (7) and the center of mass (8). Points visible in the planar view are: tip of the bill (9), base of the neck (10), mid-body (11), tip of digit IV (12), base of the tail (13), tip of the tail (14) and the center of mass (15). Points 16 and 17 in the lateral view are the points of maximum curvature of the ventral and dorsal sides of the body. With point 6, they are used to define the general slope angle of the curves of the back of the body. Also shown are the division of the body's long axis into three subunits (analyzed separately in the kinematic analysis), and the definition of the tilt angle of the tail (α_T), body (α_B) and neck (α_N), relative to the mean swimming direction (red, dotted arrows).

added mass, we use elongated body theory (Lighthill, 1970), which shows that all elliptic cross-sections from a circle to a disk with the same diameter will have an added mass approximately equal to a cylinder of the same diameter. We used a scanned planform photograph of a left foot of a bird (digit I=4.4 cm; digit IV=10.2 cm) and measured the local chord of the foot every 6 mm along its span. We then calculated the projected length of each chord in the cross-flow that results from positioning the foot at the local AoA. Next, we used each two projected lengths determining a section (6 mm wide) on the foot as diameters of a circle and calculated the volume of the section as a truncated cone. Finally, we integrated the volume of all cones to yield the mass of water moved with the foot. The virtual mass (M_α) is then the sum of the mass of the foot and the mass of the water moved with it at the specific AoA. The mass of the foot used as reference was 0.018 kg in air. We used a water density (ρ) of 10^3 kg m^{-3} to convert the volume of water to mass.

Experimental setup

Birds entered the pool (8×5 m; 1 m deep) one at a time. The pool was divided into two sections, connected through a straight 7 m-long metal mesh channel, with a rectangular 0.5×0.5 m profile, placed on the floor of the pool. The mesh of the channel was a 0.02×0.05 m grid. A door at the entrance to the channel allowed timing of the dives through the channel. The opening of the door provided the auditory and visual signal for the birds to enter the channel and swim along it until exiting from the other side and receiving a fish as a reward. A 2 m-long section of the channel, starting 3.5 m away from the entrance, was used as the test section. The position of the test section along the channel was chosen to allow sufficient distance for the birds to develop straight and uniform swimming prior to the measurement of swimming parameters. The testing section was equipped with a mirror (2×0.7 m) angled at 45° above the channel. The birds were filmed swimming in the test section using a CCTV video camera (VK-C77E; Hitachi), inside an underwater housing, connected to a S-VHS video (HR-S7600AM; JVC). The camera was positioned 0.5 m above the bottom, 2 m away from the middle of the testing section, and covered the testing section and the mirror, allowing both lateral and dorsal (through the mirror) views of the swimming bird using a single camera. The channel was positioned along the floor at the center of the pool, at least 1 m away from the nearest wall. We calculated the ground effect (Hoerner, 1975b) on the cormorants and found it to be negligible beyond a distance of one body thickness (maximum distance between dorsal and ventral sides of the body) from the floor at a Reynolds number of >10^6, and hence used only swims that were >10 cm distant from the floor. The upper 0.5 m height limitation of the channel ensured that the birds were swimming away from the surface at a distance of more than four times the body thickness. Hence, formation of surface waves by the swimming bird and the resulting added drag were considered negligible. This was also confirmed by observation of the absence of surface deformations.

Kinematics

Video sequences were converted to separate digital fields (50 fields s^{-1}) using a video editing system (Edit 6; Autodesk Inc., San Rafael, CA, USA). The data derived from each field were thus separated by a time interval of 0.02 s from the previous and next fields. The position of specific points on the birds in each field was measured using Scion Image (Scion Corp., Frederick, MD, USA). The points measured (Fig. 1B,C) were: the tip of the bill from the side (point 1 in Fig. 1) and from above (point 9), the base of the foot (joint between the tarsusmetatarsus and digits) from the side (point 4), the tip of digit IV from the side (point 5) and from above (point 12), and the base and the tip of the tail from the side (points 6, 7) and from above (points 13, 14). Two additional points at the center of the body from the lateral and dorsal view (points 3, 11) were marked by gluing (SuperWiz, Loctite glue) small round distinguishable tags (1.5 cm in diameter) onto the center of the wing facing the camera and on the back of the bird along the longitudinal midline of the body. From the glued tags and the base of the tail, four additional points were calculated trigonometrically by applying their position from the morphometric data, measured on the carcasses, relative to the digitized points (3, 6 and 11, 13). These points were the center of mass (points 8, 15) and the point of connection between the body and neck (base of neck; points 2, 10). We also digitized the point of maximum curvature of the dorsal and ventral sides of the body in the lateral view. We used these points (15, 16 in Fig. 1) and the point at the base of the tail (6) to measure the mean sloping angle of the aft (rear end) of the body. We used a Cartesian 3-D-axis system throughout the work to describe the position of the points, where X is the horizontal direction of swimming, Y is the vertical direction (height of the channel, up/down) and Z is the lateral direction (width of the channel, left/right).

Only complete paddling sequences with no significant side motions were analyzed. The sequences taken included one complete paddling cycle that followed at least three earlier cycles of horizontal straight swimming and was followed by at least another cycle of horizontal straight swimming. The points from the upper view were used to isolate straight swimming sequences where no neck turns to one side were evident (tip of bill compared with mid body point). The position of the point (11) marked on the back, relative to the frame of the channel, was used to measure the distance of the bird from the camera for scale and parallax elimination. A total of five swimming sequences for each of the nine birds was analyzed. Several sequences had an average slight vertical deviation during the cycle, i.e. the birds were swimming with a small angle to the water surface (<6°). To account for this, the mean straight path of the bird was calculated for each sequence as a straight line connecting the starting and ending position of the bird's marked point (3), and all calculations of tilting angles and positions are presented relative to this mean swimming direction. A similar procedure was applied for the upper view using point 11.

For analysis, the body length of the birds was divided into

three subunits (Fig. 1C): neck (N), body (B) and tail (T). N was defined between the points of the tip of the bill and the base of the neck, thus including the head and neck (between points 1 and 2). B was defined between the base of the neck and the base of the tail, including the folded wings (between points 2 and 6). T was defined from the base to the tip of the tail (between points 6 and 7). Using the digitized points, we measured for each field the following:

(1) tilt angle of N relative to the mean direction (α_N),

(2) tilt angle of B relative to the mean direction (α_B),

(3) tilt angle of T relative to the mean direction (α_T),

(4) the displacement of the digitized points on N, B and T in the *XY* plane (vertical) and *XZ* plane (lateral) throughout the paddling cycle,

(5) the path of the moving feet in the *XY* plane and *XZ* plane during the stroke phase.

In the kinematic analysis of the dorsal view, it was not possible to follow the base of the foot (point 4 in Fig. 1) during paddling, as it passed beneath the body and tail. For the analysis of foot motion in the *XZ* plane during the stroke, we used an additional set of video sequences, obtained separately, showing ventral views of the swimming birds during paddling. To obtain these sequences, a mirror was placed on the bottom of the channel at a 20° angle. The video camera was tilted at 50° below the horizon towards the mirror. The horizontal distance of the camera from the center of the mirror was 89 cm. The upper corners of the mirror protruded 16 cm into the channel, and the feet and ventral side of the birds were filmed at 20–40 cm above the bottom. To minimize error from parallax, due to the proximity of the camera, we measured a scale calibration factor for each of the junction points of a 5×6 cm grid placed horizontally in the channel and elevated by 5 cm between measurements. We thus calibrated a volume in the center of the mirror (55×30 cm and 20 cm high) and assigned the correct value to each digitized point based on its coordinates.

Model of hydrodynamic resistance to buoyancy

To test the hypothesis that lift from the body and tail, as well as part of the propulsive force, can be used to counter buoyancy, we used a mathematical model based on quasi-steady fluid dynamics. The compatibility and contribution of the hydrodynamic forces to vertical stability was tested by estimating the magnitude and direction of forces and comparing the resultant vertical force with buoyancy.

The lift generated by a tilted body can be calculated using the equation:

$$L = 0.5 C_L \rho A U^2 , \qquad (1)$$

where $C_L = \alpha\ \partial C_L / \partial \alpha$, ρ is the density of freshwater (10^3 kg m^{-3}), *A* is a characteristic area that equals b^2 (where *b* is body span or maximum width of the body; see Fig. 1B) and *U* is the swimming speed. $\partial C_L / \partial \alpha$ is the derivative (rate of change) of the lift coefficient (C_L) with angle of attack (α). We obtained this coefficient ($\partial C_L / \partial \alpha = 0.008$) from figs 11, 14 in chapter 19 of Hoerner (1975b), based on the characteristics of

a streamlined body with similar dimensions to the cormorant body, as reported in the Morphometrics section below (fineness ratio=3; elliptical cross-section; width to depth ratio=1.5). Substituting the measured instantaneous speed of the body and the AoA in the above equation, an estimation of the lift generated by the body during each stage along the paddling cycle can be calculated. The AoA of the body was calculated from α_B as the angle relative to the instantaneous swimming direction. For instantaneous swimming direction and speed we used the direction and magnitude of the speed vector measured as the first derivatives (Lagrange 3-points equation; Hildebrand, 1956) of the function describing the positions of point 3 (Fig. 1C) on the *X* and *Y* axes with time after data smoothing (3-points moving average).

For the lift force generated by the tail, the model (equation 1) is similar but we used values of $\partial C_L / \partial \alpha$ (0.035; from fig. 13 in chapter 18 of Hoerner, 1975b) relevant to delta wing theory and *A* as the planform area of the tail [tail length=0.178±0.006 m; span at the trailing edge= 0.086±0.004 m, values are the means ± S.E.M. from the video sequences of nine birds; aspect ratio (*AR*) is the ratio of span^2/wing area, *AR*=1]. We used the geometric area of a trapezoid with bases of 0.086 m and 0.02 m and a height of 0.0138 m as the planform area of the feathers of the tail (*A*=0.00731 m^2). The tail is trailing after the body and, as a result, the flow it encounters is affected by the streamlining of the aft of the body (Evans et al., 2002; Maybury et al., 2001; Maybury and Rayner, 2001). To calculate the actual AoA of the tail, we measured the slope between points 17 and 6 (Fig. 1C) on the dorsal side and 16 and 6 on the ventral side of the posterior tip of the body. We used the average of the two slope angles as an estimate of the direction of flow encountered by the tail and calculated the AoA as the difference between this average direction and the tilting angle of the tail. While this estimate may not be an accurate description of the actual flow over the tail, it is probably closer to reality than neglecting the effect of the body altogether.

The propulsive forces generated by the feet are mainly the result of hydrodynamic lift, hydrodynamic drag and inertia (acceleration reaction). When the foot motion has a vertical component, lift generated by the feet can be directed forward. The generated lift results in added drag (induced drag), and the generated drag and (generally) the inertia are directed in the opposite direction to the moving feet, mainly downward. Assuming that the feet may be considered as lifting surfaces (Johansson and Norberg, 2003), we used coefficients from the literature for lift ($\partial C_L / \partial \alpha = 0.06$; figs 3, 14 in chapter 17 in Hoerner, 1975b), induced drag ($C_{di} = 0.09 C_L^2$; figs 3, 4 in chapter 7 in Hoerner, 1975a) and drag at zero lift ($C_{d0} = 0.007$; fig. 2 in chapter 6 in Hoerner, 1975a) for a thin (4% thickness to span ratio) profiled, low aspect ratio (*AR*=4) wing to estimate the magnitude and direction of the force.

Lift of the feet is calculated as explained above for the body (equation 1), with the exception that the characteristic area used (*A*) is the area of the foot. Drag is calculated as: $D = D_0 + D_i$, where D_0 is the drag of the foot aligned with the direction of

motion and D_i is the induced drag due to lift when the foot is tilted at an AoA=α. The expansion of this expression is:

$$D = 0.5(C_{d0} + C_{di})\rho A U^2 . \qquad (2)$$

The force of inertia (F_i) is:

$$F_i = M_\alpha a , \qquad (3)$$

where M_α is the virtual mass of the foot at the specific AoA, as described above in the *Morphometrics of carcasses* section, and a is the acceleration of the foot calculated as the second derivative of the interpolate polynomial describing the change in position of the foot with time.

All forces were calculated for the left foot of the birds. The total force was then doubled to account for the contribution of the right foot.

Data analysis

All the swim sequences analyzed contained exactly one complete paddling cycle. However, cycle duration and the relative portion of the power and recovery phases of the cycles differed among individuals. To calculate the average tilt angles and excursions during a paddling cycle, we normalized the data for the average paddling cycle for all the birds. Each paddling cycle included three distinct phases, based on the motion of the feet relative to the body: (1) stroke, when the feet moved backwards, in the opposite direction to the moving body, and the digits were stretched; (2) glide, when the feet were stretched backwards with no movement relative to the body; and (3) recovery, when the feet and legs moved forward in the direction of the moving body and the digits were curled. The mean duration of each of the phases was calculated from all the birds, and all sequences were normalized by dividing the duration of each phase in the cycle by the mean duration of that phase. Thus, instead of using actual time units, the data are presented on a scale of 0–1 of an average paddling cycle.

In the *XY* plane (see below), we used the model developed above to calculate the magnitude and direction of forces generated by the feet during the stroke. The webbed area of the foot resembles a triangle. We chose to describe the motion of this surface in the *XY* plane using a point located at two-thirds of the distance between the base of the foot and the tip of the longest digit (points 4 and 5 in Fig. 1). This point represents the center of the hydrodynamic forces on the foot. We calculated the forces from each swimming stroke sequence using the velocity and trajectory of the feet (first derivative) and the axial accelerations (second derivative) from the translation of the foot in time using a piecewise four-points derivative equation (Hildebrand, 1956). The foot was assumed to produce propulsive forces as long as it had a positive (up) vertical component of speed. We then calculated the mean force and its variation from all the birds (*N*=9). To present the forces' direction and magnitude, we also calculated the forces on a foot trajectory that is the average of the trajectories from all the birds. Although this is not a true trajectory, we chose to present these data because they

averaged individual variation in swimming speed, paddling frequency, foot trajectory and foot size, which influences interpretation of the results. We discovered that the average trajectory of the moving foot was a circular arch and hence used this fact to calculate the direction and magnitude of speed and circumferential acceleration of the moving feet, rather than using the more general interpolation described above. We calculated the center of the circle and the radius from the points on the perimeter and calculated the tangential speeds and circumferential acceleration at each point from the change in arch length traversed with time. Since these inertia and drag forces work on the same axis as speed, and lift acts at a perpendicular angle, the direction of forces lies on the radial and tangential axes of a circular motion, presenting a simplified balance of forces. Not all foot trajectories followed a precise arc of a circle (although this was quite common); hence, the more general approach used for calculating individual sequences. At the point of transition between the recovery and the stroke phases (first field of the stroke phase), the feet may have some inertia from deceleration, although their speed is 0 m s^{-1}. We did not account for this added force at that stage since it is a consequence of the recovery phase and it is mainly in the swimming direction (horizontal) and therefore irrelevant to vertical force balance.

Statistical analysis was performed using STATISTICA (StatSoft Inc., Tulsa, OK, USA). The data set comprised five analyzed swims for each of the nine birds. To compare among birds, the means of the five runs for each bird were used (*N*=9). Significance level was set to 95% (*P*<0.05).

Throughout, error values are presented as ± standard error of the mean (S.E.M.).

Results
Morphometrics

The carcasses measured had a mean body mass of 2.215±0.04 kg and a body length of 0.81±0.003 m (*N*=88). All carcasses were positively buoyant with a mean specific weight of 0.81±0.005×10^3 kg m^{-3} (*N*=88). The mean mass-specific buoyancy was 2.3±0.07 N kg^{-1} (*N*=88). The position of the center of mass of the birds was at 54.6±0.5% (*N*=18) of the bird's length (from the tip of the bill). Underwater, however, the center of vertical static stability was posterior to this point by 2.7±0.4% (*N*=18) of the bird's length. The body (excluding neck and tail) had a fineness ratio (length-to-width ratio) of 2.8 (mean length of 33±0.6 cm; mean diameter at the point of maximum perimeter of 12±0.2 cm, *N*=21, maximum width-to-depth ratio of the body of 1.5±0.05). The webbed area (Fig. 1A) between digit IV (the longest digit=9.7±0.2 cm) and digit I (shortest digit=4.8±0.1 cm), when the digits are spread to 110° between them, was on average 4×10^{-3}±7.9×10^{-5} m^2 (*N*=22). During the stroke, the webbed area takes the shape of a swept lifting surface with a span of 12.4±0.2 cm, resulting in an aspect ratio of 3.9.

Added mass at different AoAs ranged from ~0 kg (at AoA=0) to 0.166 kg (at AoA=90°).

Kinematics of body and tail

The mean swimming speed of all the birds ($N=9$), calculated as the distance traveled in one paddling cycle divided by cycle duration, was 1.50 ± 0.03 m s^{-1} or equivalent to 1.98 ± 0.09 bird lengths s^{-1}. The mean paddling frequency was 1.60 ± 0.04 Hz. The birds used burst-and-glide swimming in all the runs. The paddling cycle consisted of three distinct phases, as described above. The mean period of a paddling cycle comprised 0.156 ± 0.003 s for the stroke phase (25%), 0.292 ± 0.031 s for the glide phase (47%) and 0.175 ± 0.008 s for the recovery phase (28%). The mean swimming speed was significantly correlated with body length ($r^2=0.77$, $P<0.02$, $N=9$).

Birds accelerated during most of the stroke phase but started decelerating toward the end of the phase, continuing to decelerate during the following glide and recovery phases (Fig. 2).

Tilting of the body, tail and neck units relative to the mean swimming direction changed distinctively during the different phases of the paddling cycle (Fig. 3). The body and tail units maintained a negative angle to the mean swimming direction throughout the entire paddling cycle (in an average sequence, the ranges of these angles were $-14.5°<\alpha_B<-6.1°$ and $-18.4°<\alpha_T<-5.2°$ for the body and tail, respectively). α_N was mostly negative but reached $0°$ at the beginning of the glide phase. During the stroke phase, the changes in α_B, α_N and α_T were rapid. The tilting angle of the body unit initially increased (α_B decreased since $\alpha_B<0$) and then decreased. By contrast, tilting of the tail initially decreased and then increased during the stroke phase. Tilting of the neck unit decreased throughout the stroke phase until the neck was aligned with the swimming direction ($\alpha_N=0$). In the following glide phase, the tilting angle of the body and the tail gradually decreased and remained fairly steady until the next stroke, except a slight increase in the tilt of the body during the recovery phase coupled with a slight decrease in the tilt of the tail. In general, the body was tilted further than the tail during the stroke and less than the tail during the glide and

recovery phases. Tilting angle of the neck gradually increased from the middle of the glide phase and during the recovery phase.

Deviations from the average straight path are presented in Fig. 4 for the center of mass and other points on the body and in Fig. 5 for the points on the neck. The mid-line of the body followed closely the mean direction of swimming in the horizontal (XZ) plane, with no visible yaw or sideslips. In the vertical (XY) plane, the center of mass descended steeply during the stroke phase, followed by a relatively moderate ascent during the longer glide and recovery phases. The base of the neck (the lowest point on the body when it is tilted at a negative angle) followed the same descent and ascent pattern as the more posterior point of the center of mass. This implies that the observed vertical excursion was not just the outcome of rotation of the body previously described (as the body performs the tilt) but rather that the entire body was descending. The vertical excursions of the base of the neck were only 2 cm on average but were in a clear consistent pattern in all the birds. The tip of the bill revealed a different moving pattern from the points on the body. It was moving in the opposite direction to that of the base of the neck during the stroke and recovery phases (Fig. 5).

The pattern created by the change in tilting angles of the body during the paddling cycle was similar in all the birds, but the absolute values of the tilting angles varied slightly among and within birds. To assess the source of variation, we tested for correlation between the mean α_B during each paddling phase and the mean swimming speed. Indeed, the mean α_B of the stroke, glide and recovery phases was weakly, but significantly, positively correlated with swimming speed ($N=45$; stroke – $r^2=0.1$, $P<0.03$; glide – $r^2=0.37$, $P<0.001$; recovery – $r^2=0.18$, $P<0.005$), indicating that in general birds that swam slower tilted their body further (a more negative α_B) and *vice versa*.

In the average paddling cycle, for the range of swimming speeds and AoAs, the lift generated by the body is in the range of 0.7–2.9 N. During the stroke phase, when body tilting is
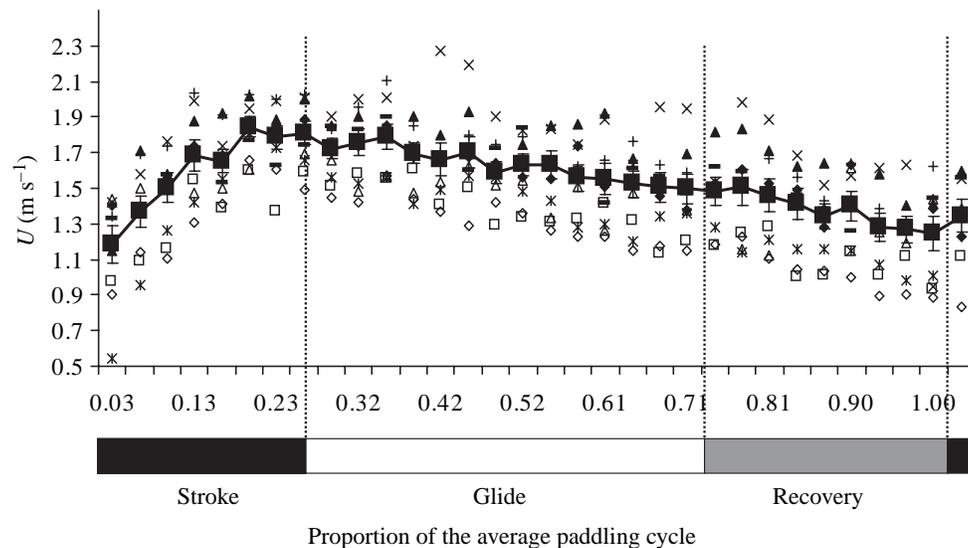

Fig. 2. The instantaneous horizontal speed (U; calculated from the displacement of point 11 in Fig. 1B) of the great cormorant during an average paddling cycle. Each symbol represents the instantaneous speed of one bird (mean of five runs). The solid line (black squares) is the mean of all birds ($N=9$). The acceleration of the body (power phase) occurs during most of the stroke phase (first six fields) followed by a deceleration until the next stroke phase. The X axis is the proportion of the cycle duration normalized by dividing the period of each phase (stroke, glide and recovery) by the mean duration of that phase (see text).
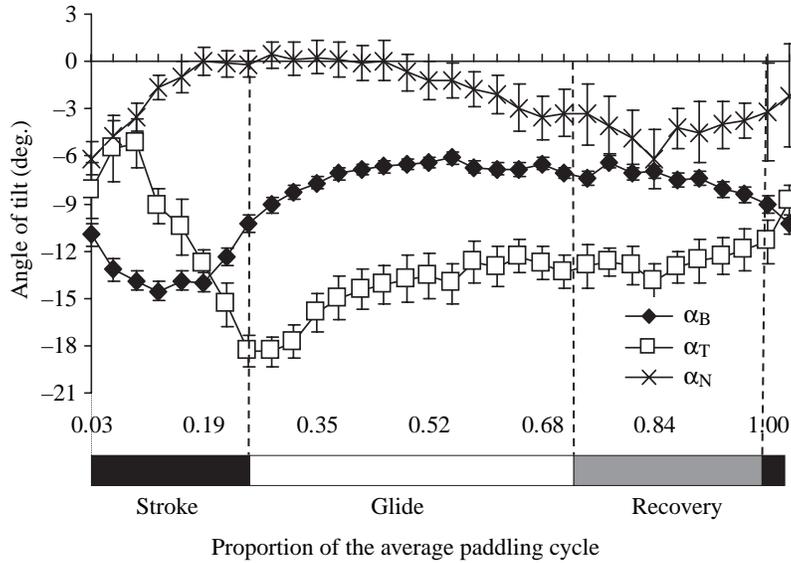
Fig. 3. Tilting angles of the body, tail and neck (α_B, α_T and α_N, respectively) during the paddling cycle of a swimming great cormorant. Angles are relative to the mean swimming direction (see text). The angles are ≤ 0 throughout the paddling cycle. α_B and α_T are in anti-phase during the stroke phase, and α_T remains at a steeper angle than α_B during the glide and recovery phases. Each data point on the curve is the mean ± S.E.M. of all birds ($N=9$). The X axis is the same as described in Fig. 2 and in the text.

maximal ($\alpha_B \ll 0$), the lift generated by the body at the instantaneous swimming speed is sufficient to offset over 60% of the buoyancy. At the end of each cycle, where the speed is low and the tilting of the body is relatively low, the body lift force still offsets 30% of the buoyancy. The mean offset of buoyancy (due to body lift) for the entire paddling cycle was 40%. The lift of the tail adds a down thrust during the glide and recovery but during the stroke it actually works in the direction of buoyancy. The total contribution of the tail to countering buoyancy (down thrust) was 13%.

Feet kinematics

During the stroke, the foot motion (as described by the positions of the center of hydrodynamic forces of the foot surface) could be divided into two stages. In the first stage (fields 1–6), the foot had a lateral (away from the midline of the body) motion in the XZ plane (Fig. 6A) and moved upward and backward. Due to the forward speed of the body, the backward motion of the foot resulted in only a small horizontal motion relative to still water (Fig. 6B). By field 4, the feet ceased to move backwards relative to the water but,
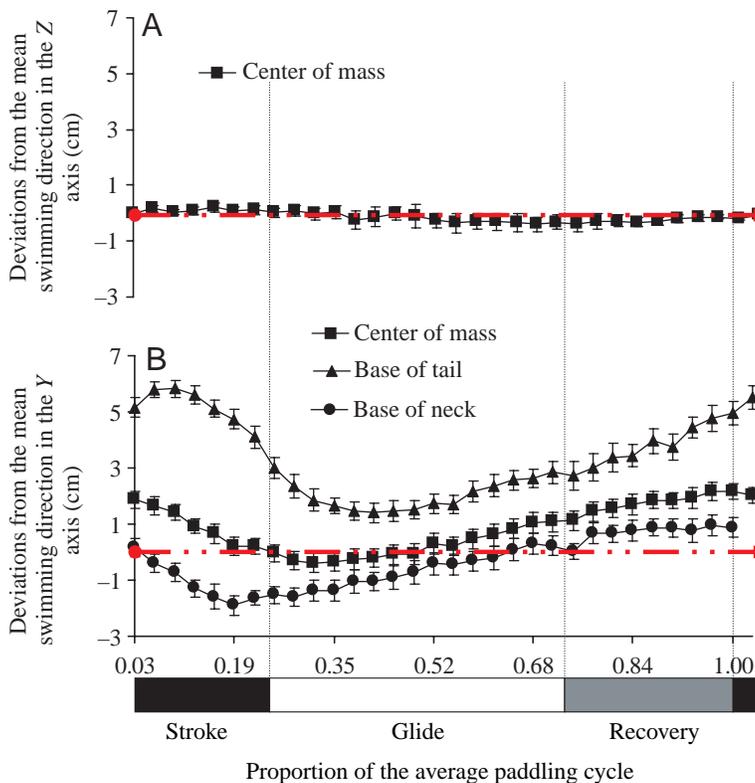

Fig. 4. The position of the digitized points representing the body of the great cormorant, relative to the mean swimming direction. (A) The center of mass of the bird demonstrated no significant deviations from the swimming direction in the Z direction (right/left). (B) Deviations in the Y direction (up/down) of three points on the body. Positive values are upward movements, and negative values are downward movements. The points are at anterior (base of neck), center (center of mass) and posterior (base of tail) locations on the body unit (points 2, 8 and 6 in Fig. 1C). All points descended during the stroke phase and ascended during the glide and recovery phases. The base of the neck (most anterior point) follows the pattern of the center of mass, indicating that the entire body is descending and ascending. The larger amplitude of the base of the tail can be attributed to the tilt of the body (rotation). The deviations are relative to the mean direction of the birds, calculated as the straight line connecting the position of point 3 in Fig. 1C (for the XY plane) or point 11 in Fig. 1B (for the XZ plane) at the beginning and end of the paddling cycle. The red broken arrows mark these directions. Each data point is the mean ± S.E.M. of all birds ($N=9$). The X axis is the same as described in Fig. 2.
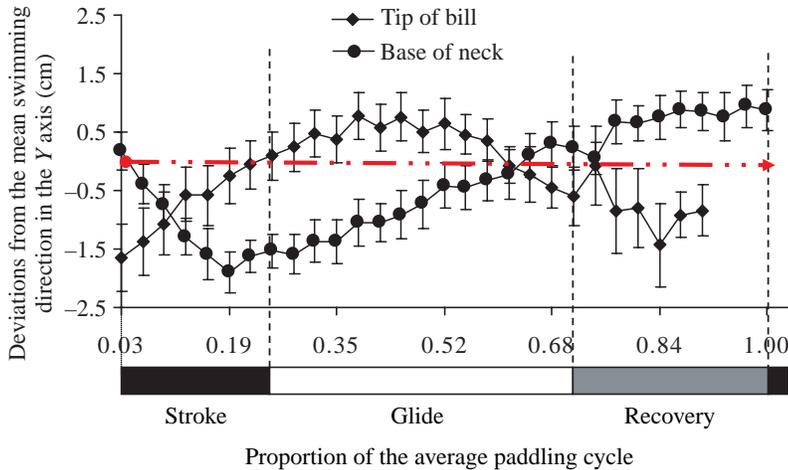
Fig. 5. Deviations in the *Y* direction (up/down) of points on the neck. The deviations are relative to the mean swimming direction of the birds (red broken arrow). The *Y* axis is the same as described for Fig. 4B, and the *X* axis is the same as described for Fig. 2. The points are the tip of the bill and the base of the neck. Several points are missing at the end of the cycle, as the birds exited the view of the camera. It is clear, however, that the tip of the bill moves differently from the body (represented by the base of the neck), ascending when the body descends during the stroke phase and *vice versa* during the end of the glide and the recovery phase.

in fact, continued moving backward relative to the body up to field 6 (Fig. 7), at which point the vertical motion of the foot also ended. In the second stage (fields 6–8), the foot had only a medial motion (towards the midline of the body) while following the body in the vertical (*Y*) and horizontal (*X*) directions (Figs 6, 7). This stage was associated with digit abduction (closure) as the overall planar area of the webbed feet decreased. The second stage, therefore, contributed little or any to the thrust of the bird, an assumption that was corroborated by the fact that the instantaneous speed of the birds decreased after field 6 (Fig. 2). The first stage of the stroke is thus the power phase of the paddling cycle (the phase when thrust is applied). During the recovery phase, the feet moved forward, parallel to the midline of the body, with no visible lateral motions. Since, during the effective part of the stroke, both feet move laterally in opposite directions, the lateral forces will cancel each other out, leaving only the thrust component that is directed in the *XY* plane. Hence, our analysis focuses on the *XY* plane, where pitch moments and vertical adjustments are more likely to take place.

The back-sweep motion of the foot followed roughly the contour of the ventral side of the body. Since the body was at maximal tilt during the stroke, the feet were further directed upward during most of the stroke phase (Fig. 7). An analysis of the AoA of the webbed area of the feet compared with the foot trajectory (Fig. 8) shows that the drag and inertia generated by the moving feet are directed mostly downward, in the opposite direction to the moving feet. However, the lift generated by the AoA of the feet would act towards the center of the circle that forms the trajectory arch (Fig. 8). The lift, drag and inertia forces, generated by the moving feet in the *XY* plane, are directed mainly at a downward angle relative to the swimming direction. The overall propulsive force (resultant vector) is therefore directed below the actual swimming direction, thus actively offsetting buoyancy.

Fig. 9 describes the model's prediction of magnitude and direction of the resultant propulsive force generated by the
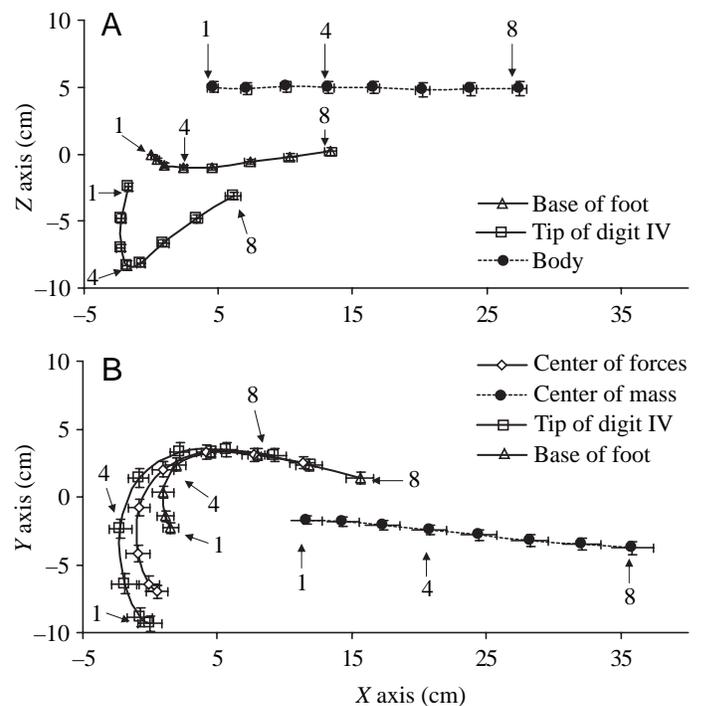

Fig. 6. Foot kinematics (left foot) of the great cormorant during the stroke phase, relative to still water. Points shown are the base of the foot and the tip of digit IV (points 4 and 5 in Fig. 1) and a reference point on the body (filled circle). Swimming direction is left to right. (A) The motion in the *XZ* plane during an average stroke. The position of the body is represented by a point on the ventral body mid-line. (B) The motion in the *XY* plane of points 4 and 5 of Fig. 1 and the center of hydrodynamic forces of the foot, located at two-thirds of the distance between points 4 and 5 (see text). The body is represented by the center of mass (point 8 in Fig. 2). Numbers adjacent to data points denote field numbers (fields are separated by 0.02 s intervals, starting at 1 as the first field of the stroke phase). The two views (*XZ*, *XY* planes) are averages analyzed from different paddling sequences due to limitations of the setup (see text). The two sequences were synchronized by matching the first fields of the stroke phase and resetting the values on the *X* axis in the first fields of the stroke phase.
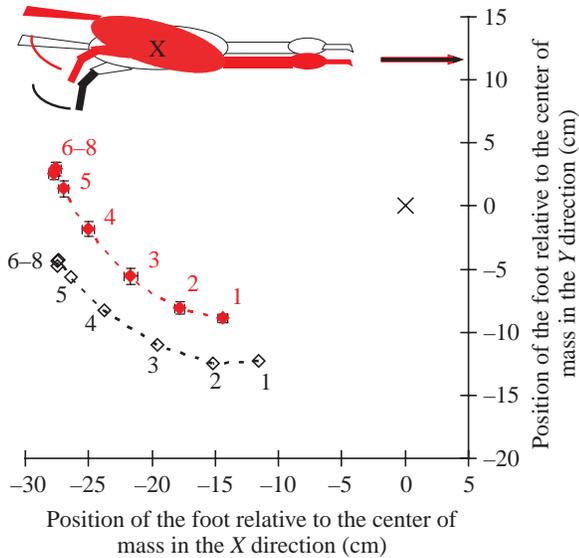
Fig. 7. The back-sweep arch of the foot of the great cormorant, relative to the body, in the *XY* plane (red symbols). The surface of the foot is represented by the center of hydrodynamic forces (see text). Each point is the mean from all birds (*N*=9). The points shown belong to the stroke phase and are spaced by 0.02 s intervals (the time frame between fields) and sequenced by the adjacent numbers. The position of the foot is presented relative to the position of the center of mass located at point (0,0) and marked by '×'. The bird swimming direction is from left to right. During the stroke phase, the body is at maximal tilt, as indicated by the orientation of the red figure. The arch of the foot trajectory is vertical, partly due to the fact that the body is tilted. The vertical motion relative to the center of mass is in the first 0.12 s of the stroke phase (fields 1–6). The white open symbols are the same data as the red but rotated at 15° counterclockwise to demonstrate a hypothetical foot trajectory when the cormorant body aligns with the swimming direction (orientation of the white figure).
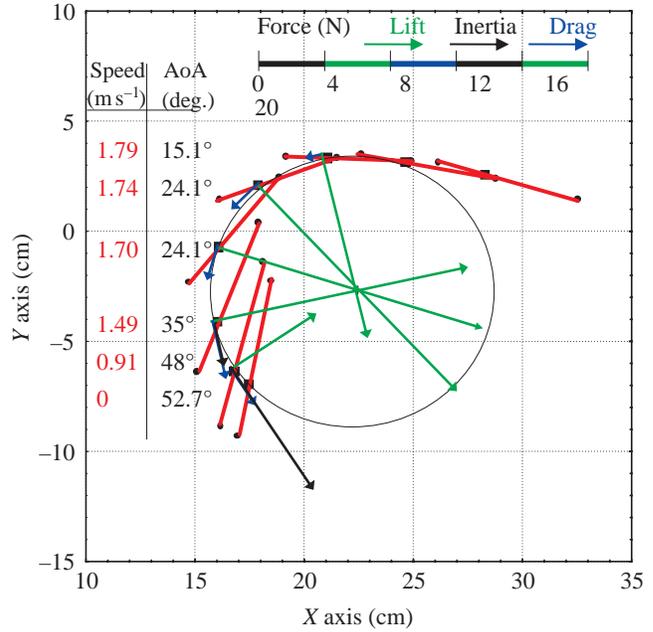

Fig. 8. An analysis of the average trajectory of the foot of the great cormorant relative to still water and the resulting hydrodynamic forces (the same data as in Figs 6, 7). Black squares mark the position of the center of hydrodynamic forces of the foot in the *XY* plane. The positions of this point were used to calculate the trajectory, speed and angle of attack (AoA) of the foot. Red lines connect between points 4 and 5 in Fig. 1 and represent the webbed surface of the foot in the *XY* plane, demonstrating the AoA between this surface and the foot trajectory. The motion relative to still water, calculated for the center of hydrodynamic forces, fitted a circle (black line) with a radius of 6.6 cm. The speed (red) and the AoA (black) are aligned with each relevant point in the table to the left. Motion starts from the bottom and follows the arch of the circle up. The values of AoA and speed are organized in bottom-to-top order as well. Lift forces (green arrows) will be directed at a perpendicular angle to the foot trajectory and, in this case, toward the center of the circle. Drag (blue) is directed at the opposite direction to the motion of the feet, and in this case the inertial force (black) is in the same direction as drag. Forces smaller than 0.5 N were omitted from the figure.

cormorant (both feet) in the *XY* plane during the power phase (fields 1–6). The forces in each field are the averages of all the birds. It serves to show that the overall thrust generated by the feet (drag, inertia and lift) is directed well below the swimming direction (the resultant vector of thrust being directed at –44°). Thus, the thrust generated by the feet in the *XY* plane serves equally to produce forward motion and to counter buoyancy.

Fig. 10 summarizes the net vertical forces produced by the lift of the body and tail and the vertical forces of the foot. The vertical component of the propulsive forces of the feet during the stroke phase exceeds the buoyancy and the positive lift of the tail. This results in the downward motion of the body during the stroke phase and in the up-drift during the glide and recovery phases. For the entire paddling cycle, the vertical component of the propulsive force counters 32% of the buoyancy. Combining the vertical forces of the lift from the body and tail and from the forces of the feet, the vertical force offsets for the entire paddling cycle are about 85% of the positive buoyancy.

Discussion

The cormorants, swimming in the shallow pool, demonstrated a clear pattern of body tilting as part of their swimming mode. The fact that this pattern was coupled with vertical adjustments of the swimming trajectory suggests that the role of body tilting is to aid in offsetting the up-drift caused by the positive buoyancy. Up-drift was observed during the glide and recovery phases, where no propulsive force was produced, whereas down-drift occurred during the stroke phase. Body tilting may offset buoyancy by two different, yet not mutually exclusive, mechanisms. In the first, the tilted body, moving through the water, generates a hydrodynamic lift force, which is proportional to the AoA. Since the tilting angle of the body creates a negative AoA, the resulting lift will push the body downward, working against buoyancy. The use of this

mechanism is also supported by the positive correlation between α_B and the swimming velocity, which results in a greater lift coefficient when the velocity is low. Such a use of the body has been speculated upon in the past by various authors, with no quantitative proof, based on the body shape as measured by Lovvorn et al. (2001). In the second mechanism, body tilting positions the body in a more vertical direction, providing a larger vertical component to the back-sweep arch of the feet and hence directing the thrust forward, at a downward angle relative to the actual swimming direction.
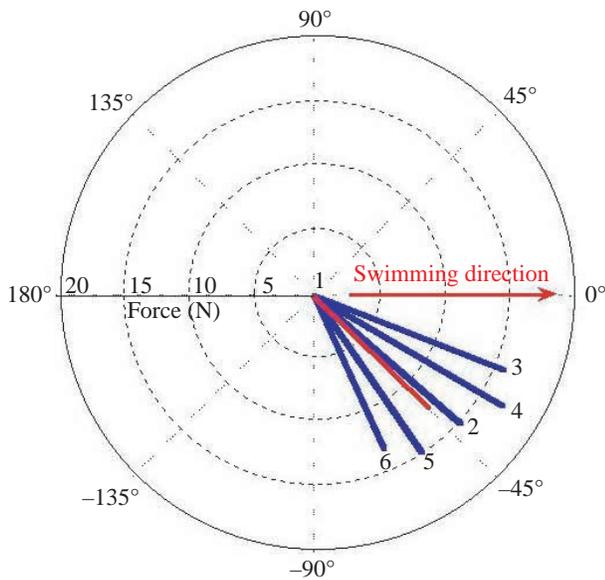
Field	S.E.M. magnitude (N)	S.E.M. direction (deg.)
1	0	0
2	3.3	19.7
3	2.0	7.5
4	2.5	13.0
5	2.0	11.4
6	2.3	17.4

Fig. 9. The propulsive forces (drag, lift and inertia combined) generated by the feet of the great cormorant during the stroke phase (fields 1–6). Each blue line is the mean force vector from all the birds for a specific field. Fields are separated by 0.02 s time intervals and sequenced by adjacent numbers. Forces' magnitude and direction are estimated according to the model (see text) using low aspect ratio wing calculations. Values include the forces of both feet. The overall propulsive force (the resultant vector of fields 1–6; in red) is directed at 44° below the actual swimming direction of the birds, thus contributing a large vertical component to aid in resisting buoyancy. The model accounts for motion in the *XY* plane and disregards the contribution of lateral motion. The red arrow is the swimming direction of the birds. Variation (S.E.M.) of the vectors' direction and magnitude is mentioned in the table.

This means that the propulsive force has a larger vertical component directed at resisting buoyancy. In the case of our shallow-swimming birds, both mechanisms seem to apply, since the body tilted to a maximum and descended during the stroke phase but maintained a negative AoA throughout the following glide and recovery phases. This form of dynamic buoyancy control may also apply to other diving animals with high positive buoyancy. Dynamic buoyancy control, as opposed to hydrostatic control, is better suited to fast changes in buoyancy of the animal during the dive (increase in dive depth, release of air from the plumage/fur). In birds, dynamic control has a further advantage since birds are buoyant as a consequence of adaptation to aerial flight. By using dynamic buoyancy control, birds can counter buoyancy without increasing the cost of aerial flight. However, they pay an energetic toll during swimming due to increased drag and due to assigning part of the propulsive force vertically.

It seems that by simply tilting their body and tail, the cormorants can roughly halve the effect of buoyancy while swimming horizontally. This implies an interesting fact: since the buoyancy of birds is mainly the result of compressible air volume, the reduction in the up-thrust due to body and tail lift is equivalent to diving at a depth of approximately 10 m. This depth is well within the diving range of cormorants and is close to the median dive depth of 6.1 m reported for free-ranging great cormorants by Gremillet et al. (1999) or to the average dive depth (10.2 m) according to Ross (1977) (cited in Johansgard, 1993). Since tilting of the body affects both the lift of the body and tail and the vertical component of the propulsive force, it would be interesting to see if the horizontal swimming of cormorants is optimized for a depth of ~10 m, at which α_B can be close to zero during the glide, thus reducing body drag and hence increasing the distance traveled per paddling cycle.

It is evident, however, that lift from the body and tail *per se* is not enough to cancel out buoyancy at 1 m depth. Therefore, the cormorant must invest propulsive energy directly to resist up-thrust.

Cormorants propel themselves through the water by sweeping their feet along an arch extending from an anterior point along the body's main axis to a posterior point underneath the tail. The symmetry of the lateral motions of the feet cancel out the lateral forces (as demonstrated by the fact that the birds swim with no side-slip), and the net propulsive force is in the *XY* plane. Our results are in agreement with Johansson and Norberg (2003) regarding feet trajectory and AoA, further indicating that the large vertical component of the feet trajectory may be increased by the tilting angle of the body and thus involved in buoyancy offset. Hence, by tilting the body at varying angles to the swimming direction, the cormorant can shift the direction of the overall thrust to give priority to resisting buoyancy or to forward motion.

Our estimates of the vertical forces accounted for 85% of the buoyancy of the carcasses. This small discrepancy can be explained by a combination of underestimation of the forces by using lift and drag coefficients obtained for rigid, smooth
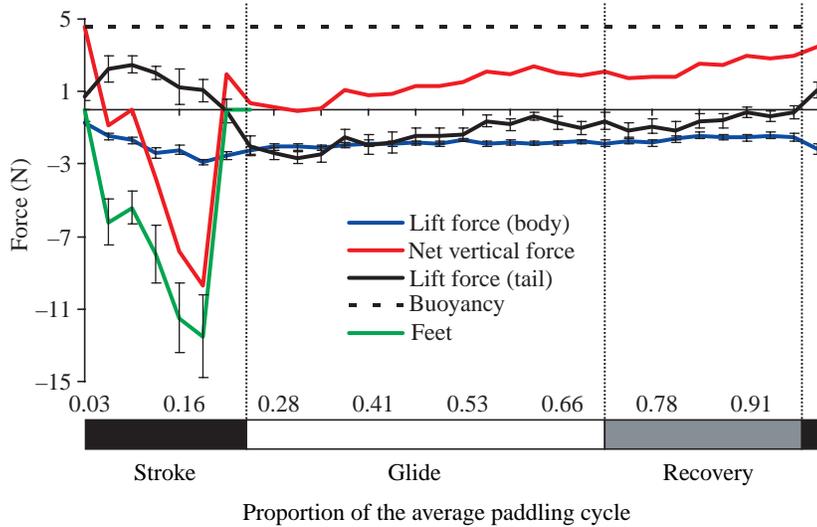
Fig. 10. The contribution of hydrodynamic forces to buoyancy offset during the entire paddling cycle. Presented are the vertical components of hydrodynamic lift from the body (blue line) and from the tail (black line) and the vertical forces generated by the feet (green line), as calculated by the model described in the text. Values are the means ± S.E.M. of all birds (*N*=9). Also shown is the average buoyancy estimated from measurements on the carcasses (broken line). The net vertical force (red line) is calculated by subtracting the value of the vertical hydrodynamic forces from the positive buoyancy of the carcasses. The *X* axis is as described in Fig. 2.

technical models and of overestimation of the buoyancy of the birds from the measurements on carcasses.

An interesting point regarding cormorant propulsion is that during the stroke the feet are rotated mainly around the tarsusmetatarsus–tarsustibia (TMT–TT) joint. The knee and the hip joints have a much reduced range of motion due to skin and muscle tissue and due to the large patella (Johansgard, 1993). The TMT–TT joint allows almost a 180° rotation of the TMT around the TT, as evident when the birds are examined by hand or when wild birds are observed perching on trees. Throughout our experiment, however, the swimming cormorants seldom rotated the TMT about the TT in an angle exceeding 90°. The reason for this behavior is unclear and may have an anatomical explanation. However, the outcome of this limited bending of the joint to an angle of 90° is that the range of motion during the stroke is mainly in the vertical direction and, to a much lesser extent, in the horizontal direction. Bending the joint to its maximum would allow the feet a further thrust forward that is drag based (Fig. 7). However, it will also create a low drag (and optionally lift) component directed upward and even more so when the bird's body is aligned with the swimming direction. It is possible that cormorants bend their TMT–TT only to 90° to avoid this vertical component. For lift-based forward thrust, the feet need to move perpendicular to the direction of the moving body. A 90° rotation of the TMT about the TT, while the body aligns with the swimming direction, uses only half of the vertical arch of a circle. Tilting of the body further shifts this arch to a more vertical trajectory (Fig. 7).

The cormorant's use of lift for propulsion in the back of the body and the vertical motions of the propelling appendages slightly resemble the swimming of marine mammals. However, while cetaceans generate thrust by moving their tails up and down, the power phase of the cormorant utilizes thrust from motion in only one direction (up). The symmetrical vertical excursions of the dolphin swimming (when repeated at equal speeds) cancel out, leaving a mainly horizontal component of the propulsive force (Fish, 1993). Our cormorants seem to use a different tactic, as their asymmetrical paddling in the vertical direction (only upward) is balanced by their high buoyancy, resulting in the vertical drift pattern reported herein. This solves the problem of high buoyancy, on the one hand, and allows the utilization of lift for forward thrust from vertical motions of the feet, on the other hand.

The cormorant's tail moves separately from the rest of the body and serves as a control surface, determining the tilting angle of the body throughout the paddling cycle. During the end of the recovery phase and the following stroke phase, the tilting angle of the tail changed in anti-phase with the angle of the body, supporting the notion that it regulates and probably generates the tilting angle of the body. During the end of the glide, the angle of the body was kept approximately constant (and so was the steeper angle of the tail), suggesting that a static pitching moment of the body was countered by the dynamic pitching moment generated by the tail. This was corroborated by the position of the center of vertical static stability measured from the carcasses. This position was always slightly posterior to the center of mass, meaning that the carcass was not statically stable and hence the body has a tendency to tilt with the back of the body rising. While swimming, the tail's posterior position and lift-generating geometry seems to offset and control these pitching moments on the body, pushing down against the tendency of the back of the body to tilt during the glide and during the beginning of the recovery phase. During the stroke, the tail allows and initiates the pitch of the body, forming the swimming pattern described herein. Only a few water birds have developed tails to the extent of those of cormorants and anhingas. The tail feathers of the measured carcasses in the present study constituted 22±0.2% (*N*=88) of the body length (from the tip of the bill to the tip of the longest tail feather). They also comprise an area of 18.7±0.2% of the planar area of the body + tail as measured from carcasses (*N*=5). The important role we find for the tail in controlling pitch moments and thus in offsetting buoyancy may explain the success of these aquatic predators in varying foraging sites, both shallow and deep. The

shape and function of birds' tails during flight has been widely debated recently (Evans and Thomas, 1992; Hedenstrom, 2002; Maybury and Rayner, 2001; Maybury et al., 2001). It is generally assumed that the tail helps in maneuvering, lift generation and drag reduction. Here, the tail seems to serve an additional function. Unlike flying, during diving the propulsion of the body is generated at a posterior point to the center of mass (Figs 6, 7) and the propulsive force generated has a vertical component. This, combined with the fact that, underwater, the center of vertical static stability is posterior to the center of mass implies that pitching moments working on the cormorant during horizontal swimming are substantial.

The neck and head also moved in antiphase with the rest of the body. We speculate that these motions serve primarily in aligning the head in the general direction of swimming as the body tilts. The function of such a behavior can be to reduce drag on the head. These motions may also contribute to stabilizing pitch moments; however, the laterally compressed shape of the head and bill suggests that this added role, if it exists, is of minor significance. Alternative suggestions (unrelated to hydrodynamics) include visual performance and maintaining balance (Katzir et al., 2001; Warrick et al., 2002).

The tilting of the body during the stroke phase serves to counteract buoyancy. However, the birds pay an energetic toll for such a behavior. With an increase in the AoA, the drag of the body increases, resulting in an increase in the cost of transport. Since the steeper AoAs of the body are performed during the stroke phase, when swimming speed is high, this is the phase when the bird's body generates the highest drag. To reduce this added cost, the cormorants use a burst-and-glide swimming pattern. In the shallow dives analyzed herein, the average stroke phase lasted only 25% of the paddling cycle. Burst-and-glide can result in significant energy saving relative to sustained swimming, when propulsion increases the drag of the body relative to gliding (Weihs, 1974). This condition seems to apply to the tilting behavior of the cormorants.

Our trained cormorants were swimming in the experimental setup at speeds and stroke frequencies similar to those previously reported (Ancel et al., 2000; Gremillet et al., 1999; Johansgard, 1993; Schmid et al., 1995) and did not show any difficulty in performing the shallow horizontal dives. Cormorants in the wild may avoid high buoyancy by diving several meters below the surface. However, there is a physiological and ecological cost for utilizing only deeper water. The fact is that free-ranging cormorants in general, and *P. carbo sinensis* in particular, often dive in shallow lakes and fish ponds (Gremillet et al., 1998, 1999; Gremillet and Wilson, 1999). The mechanisms detailed herein aid cormorants to cope with the high buoyancy while foraging in shallow dive sites, increasing the range of diving sites and depths utilized for efficient foraging.

References

Alexander, R. McN. (1968). *Animal Mechanics*. Seattle: University of Washington Press.

Alexander, R. McN. (1990). Size speed and buoyancy adaptations in aquatic animals. *Am. Zool.* **30**, 189-196.

Ancel, A., Starke, L. N., Ponganis, P. J., Van Dam, R. and Kooyman, G. L. (2000). Energetics of surface swimming in Brandt's cormorants (*Phalacrocorax penicillatus brandt*). *J. Exp. Biol.* **203**, 3727-3731.

Baudinette, R. V. and Gill, P. (1985). The energetics of flying and paddling in water: locomotion in penguins and ducks. *J. Comp. Physiol. B* **155**, 373-380.

Boldreghini, P., Santolini, R., Volponi, S., Casini, L., Montanari, F. L. and Tinarelli, R. (1997). Variation in the use of foraging areas by a cormorant *Phalacrocorax carbo* wintering population: a case study in the Po delta. *Ekol. Pol.* **45**, 197-200.

Boyd, I. L. (1997). The behavioural and physiological ecology of diving. *Trends Ecol. Evol.* **12**, 213-217.

Butler, P. J. (2001). Diving beyond the limits. *News Physiol. Sci.* **16**, 222-227.

Butler, P. J. and Woaks, A. J. (1979). Change in heart rate and respiratory frequency during natural behaviour of ducks, with particular reference to diving. *J. Exp. Biol.* **79**, 283-300.

Domning, D. P. and Buffrénil, V. (1991). Hydrostasis in the sirenia: quantitative data and functional interpertations. *Mar. Mamm. Sci.* **7**, 331-368.

Evans, M. R. and Thomas, A. L. R. (1992). The aerodynamic and mechanical effects of elongated tails in the scarlet-tufted malachite sunbird: measuring the cost of handicap. *Anim. Behav.* **43**, 337-347.

Evans, M. R., Rosen, M., Park, K. J., Henderstrom, A. (2002). How do birds' tails work? Delta wing theory fails to predict tail shape during flight. *Proc. R. Soc. Lond. B* **269**, 1053-1057.

Fish, F. E. (1993). Power output and propulsive efficiency of swimming bottlenose dolphins (*Tursiops truncatus*). *J. Exp. Biol.* **185**, 179-193.

Fish, F. E. (2000). Biomechanics and energetics in aquatic and semiaquatic mammals: platypus to whale. *Physiol. Biochem. Zool.* **73**, 683-698.

Fish, F. E., Smelstoys, J., Baudinette, R. V., Reynolds, P. S. (2002). Fur does not fly, it floats: buoyancy of pelage in semi-aquatic mammals. *Aquat. Mamm.* **28**, 103-112.

Gremillet, D., Argentin, G., Schulte, B. and Culik, B. M. (1998). Flexible foraging techniques in breeding cormorants *Phalacrocorax carbo* and shags *Phalacrocorax aristotelis*: benthic or pelagic feeding? *Ibis* **140**, 113-119.

Gremillet, D., Wilson, R. P., Storch, S. and Gary, Y. (1999). Three dimensional space utilization by a marine predator. *Mar. Ecol. Prog. Ser.* **183**, 263-273.

Gremillet, D. and Wilson, R. P. (1999). A life in the fast lane: energetics and foraging strategies of the great cormorant. *Behav. Ecol.* **10**, 516-524.

Hedenstrom, A. (2002). Aerodynamics, evolution and ecology of avian flight. *Trends Ecol. Evol.* **17**, 415-422.

Hildebrand, F. B. (1956). *Introduction to Numerical Analysis*. New York: McGraw-Hill, Inc.

Hochscheid, S., Bentivegna, F. and Speakman, J. R. (2003). The dual function of the lung in chelonian sea turtles: buoyancy control and oxygen storage. *J. Exp. Mar. Biol. Ecol.* **297**, 123-140.

Hoerner, S. F. (1975a). *Fluid-Dynamic Drag*. S. F. Hoerner.

Hoerner, S. F. (1975b). *Fluid-Dynamic Lift*. S. F. Hoerner.

Hustler, K. (1992). Buoyancy and its constraints on the underwater foraging behaviour of the reed cormorants *Phalacrocorax africanus* and darters *Anhinga melanogaster*. *Ibis* **134**, 229-236.

Johansgard, P. A. (1993). *Cormorants, Darters and Pelicans of the World*. Washington: Smithsonian Press.

Johansson, L. C. and Lindhe Norberg, U. M. (2000). Asymmetric toes aid underwater swimming. *Nature* **407**, 582-583.

Johansson, L. C. and Lindhe Norberg, U. M. (2001). Lift based paddling in diving grebe. *J. Exp. Biol.* **204**, 1687-1696.

Johansson, L. C. and Norberg, R. A. (2003). Delta-wing function of webbed feet gives hydrodynamic lift for swimming propulsion in birds. *Nature* **424**, 65-68.

Jones, D. R., Furilla, R. A., Heieis, M. R. A., Gabbott, G. R. J. and Smith, F. M. (1988). Forced and voluntary diving in ducks: cardiovascular adjustments and their control. *Can. J. Zool.* **66**, 75-83.

Kato, A., Watanuki, Y., Nishiuni, I., Kuroki, M., Shaughnessy, P. and Naito, Y. (2000). Variation in foraging and parental behaviour of king cormorants. *Auk* **117**, 718-730.

Katzir, G., Schechtman, E., Carmi, N. and Weihs, D. (2001). Head stabilization in herons. *J. Comp. Physiol. A* **187**, 423-432.

Lighthill, M. J. (1970). Aquatic animal propulsion of high hydromechanical efficiency. *J. Fluid Mech.* **44**, 265-301.

Lovvorn, J. R. (1991). Mechanics of underwater swimming in foot-propelled diving birds. *Proc. Int. Ornithol. Congr.* **20**, 1868-1874.

Lovvorn, J. R., Croll, D. A. and Liggins, G. A. (1999). Mechanical versus physiological determinants of swimming speeds in diving Brunnich's guillemots. *J. Exp. Biol.* **202**, 1741-1752.

Lovvorn, J. R. and Jones, D. R. (1991). Body mass, volume, and buoyancy of some aquatic birds and their relation to locomotor strategies. *Can. J. Zool.* **96**, 2888-2892.

Lovvorn, J. R. and Jones, D. R. (1994). Biomechanical conflicts between adaptation for diving and aerial flight in estuarine birds. *Estuaries* **17**, 62-75.

Lovvorn, J. R., Jones, D. R. and Blake, R. W. (1991). Mechanics of underwater locomotion in diving ducks: drag, buoyancy and acceleration in a size gradient of species. *J. Exp. Biol.* **159**, 89-108.

Lovvorn, J. R., Liggins, G. A., Borstad, M. H., Calisal, S. M. and Mikkelsen, J. (2001). Hydrodynamic drag of diving birds: effect of body size, body shape and feathers at steady speeds. *J. Exp. Biol.* **204**, 1547-1557.

Maybury, W. J. and Rayner, J. M. V. (2001). The avian tail reduces body parasite drag by controlling flow separation and vortex shedding. *Proc. R. Soc. Lond. B* **268**, 1405-1410.

Maybury, W. J., Rayner, J. M. V. and Couldrick, L. B. (2001). Lift generation by the avian tail. *Proc. R. Soc. Lond. B* **268**, 1443-1448.

Ross, R. K. (1977). A comparison of the feeding and nesting requirements of the great cormorant (*Phalacrocorax carbo* L.) and the double-crested cormorant (*P. aurius* Lesson) in Nova Scotia. *Proc. Nov. Scot. Inst. Sci.* **27**, 112-114.

Sato, K., Naito, Y., Kato, A., Niizuma, Y., Watanuki, Y., Charrassin, J. B., Bost, C. A., Handrich, Y. and Le Maho, Y. (2002). Buoyancy and maximal diving depth in penguins: do they control inhaling air volume? *J. Exp. Biol.* **205**, 1187-1197.

Schmid, D., Gremillet, D. J. H. and Culik, B. M. (1995). Energetics of underwater swimming in the great cormorant (*Phalacrocorax carbo sinensis*). *Mar. Biol.* **123**, 875-881.

Stephenson, R. (1993). The contribution of body tissues, respiratory system, and plumage to buoyancy in waterfowl. *Can. J. Zool.* **71**, 1521-1529.

Stephenson, R., Lovvorn, J. R., Heieis, M. R. A., Jones, D. R. and Blake, R. W. (1989). A hydromechanical estimate of the power requirements of diving and surface swimming in lesser scaup (*Aythya Affinis*). *J. Exp. Biol.* **147**, 507-519.

Taylor, M. A. (1994). Stone, bone or blubber? Buoyancy control strategies in aquatic tetrapods. In *Mechanics and Physiology of Animal Swimming* (ed. L. Maddock, Q. Bone and J. M. V. Rayner), pp. 151-161. Cambridge: Cambridge University Press.

Wanless, S., Harris, M. P. and Morris, J. A. (1992). Diving behaviour and diet of the blue-eyed shag at South Georgia. *Polar Biol.* **12**, 713-719.

Warrick, D. R., Bundle, M. W. and Dial, K. P. (2002). Bird maneuvering flight: blurred bodies, clear heads. *Integ. Comp. Biol.* **42**, 141-148.

Webb, P. W. and Weihs, D. (1983). *Fish Biomechanics*. New York: Praeger.

Webb, P. M., Crocker, D. E., Blackwell, S. B., Costa, D. P. and Boeuf, B. J. (1998). Effects of buoyancy on the diving behavior of northern elephant seals. *J. Exp. Biol.* **201**, 2349-2358.

Webb, P. W. and Weihs, D. (1994). Hydrostatic stability of fish with swim bladder: not all fish are unstable. *Can. J. Zool.* **72**, 1149-1154.

Weihs, D. (1974). Energetic advantages of burst swimming of fish. *J. Theor. Biol.* **48**, 215-229.

Wilson, R. P., Hustler, K., Ryan, P. G., Burger, A. E. and Noldeke, E. C. (1992). Diving birds in cold water: do Archimedes and Boyle determine energetic costs? *Am. Nat.* **140**, 179-200.